Proceedings of IMECE 2002
ASME International Mechanical Engineering Congress & Exposition
November 17-22, 2002, New Orleans, Louisiana

Paper No IMECE 2002-HT-32111

MARANGONI AND VARIABLE VISCOSITY PHENOMENA IN PICOLITER SIZE SOLDER DROPLET DEPOSITION

M. Dietzel **S. Haferl**

Y. Ventikos **D. Poulikakos**

Laboratory of Thermodynamics in Emerging Technologies
Institute of Energy Technology, Department of Mechanical and Process Engineering
Swiss Federal Institute of Technology

ABSTRACT

This numerical investigation studied the effects which the temperature dependence of surface tension (Marangoni phenomenon) and viscosity has on the spreading, the transient behavior and final post-solidification shape of a molten Sn63Pb solder droplet deposited on a flat substrate. A Lagrangian finite element formulation of the complete axisymmetric Navier-Stokes equations was utilized for the description of the droplet behavior. Linear temperature dependence for the surface tension and an exponential dependence for the viscosity were assumed. The initial droplet temperature was varied in 50K steps from 200ºC to 500ºC, whereas the substrate temperature was kept constant at 25ºC. This varied the initial Reynolds number Re_0 from 360 to 716 and the Marangoni number Ma from –9 to –49. The initial Weber number We_0 and initial Prandtl number Pr_0 were for all cases O(1) and O(10^{-2}), respectively. The impact velocity and the droplet diameter remained unchanged in all cases examined at 1.5 m/s and 80 microns.

A major finding of the work was that, contrary to intuition, the Marangoni effect decreased droplet spreading monotonically. Due to the Marangoni effect, surface tension forces instead of freezing arrested spreading. Droplet receding during recoiling was aided by the Marangoni effect. On the other hand, the change of viscosity with temperature showed no significant influence on the outcome of the droplet impact.

INTRODUCTION

Free surface flows with thermal transport play an important role in a wide range of modern technical applications, such as spray deposition, injection, casting, welding, soldering or extrusion processes, Maronnier and Picasso *et al.* [1]. In recent years, there has been an increasing interest in micro-scale liquid transport with many applications in MEMS and microelectronics manufacturing.

In this context, the deposition of molten picoliter size solder droplets with diameter O(100μm) upon a flat conductive substrate was examined, thereby laying the focus on the effects of a temperature dependence of surface tension (temperature-induced Marangoni effect) and viscosity.

Earlier numerical and experimental investigations have shown that the impact velocity and surface tension are important parameters determining the fluid mechanical behavior of the droplet upon impact within the parametric domain of solder jetting processes, [2,3]. The low impact velocities of O (1m/s) ensure that no splashing occurs. Considering the importance of surface tension for the problem, a variable surface tension may change the spreading behavior of the droplet markedly.

Marangoni convection was shown to be of crucial importance in solidification processes leading to phase separation or to local concentration changes in alloys, Cao and Wang *et al.* [4]. Song and Dailey *et al.* [5] reported that internal droplet flows are often caused by surface tension forces rather than by buoyancy forces. Ehrhard and Davis [6] discussed the spreading of droplets on a horizontal plate under the presence of thermocapillary forces based on the lubrication theory. This work was extended by Braun and Murray *et al.* [7] to account for solutal Marangoni effects in Pb-Sn alloy droplets with Ma of O(10^{-1}) – O(10^{-2}). Both investigations reported a reduced spreading if the droplet was heated from the substrate underneath. The accurate prediction in spreading is of importance in many applications in microchip manufacturing. To the best of our knowledge no work on inertia dominated droplet impact flow combined with Marangoni convection has yet been presented in the open literature, a problem which typically occurs in solder jetting.

The numerical approach herein is based on the Lagrangian formulation of the axisymmetric, unsteady Navier-Stokes equations, and the energy equation, which are discretized utilizing the Galerkin finite element method and a deforming, non-adaptive triangulation mesh. The implementation employed extends the methodology of [2] to account for the temperature dependence of the surface tension and viscosity.

NOMENCLATURE

c	Speed of sound	[m/s]	α	Thermal diffusivity	[m^2/s]
d	Droplet diameter	[m]	δ	Kronecker symbol	[-]
g	Gravity	[m/s^2]	ε	Navier-slip coefficient	[-]
H, $\overline{H}$	Curvature	[1/m], [-]	γ	Surface tension	[N/m]
k	Thermal conductivity	[W/mK]	μ	Dynamic viscosity	[kg/ms]
L	Latent heat	[J/kg]	ρ	Density	[kg/m^3]
M	Mach number	[-]			
Ma	Marangoni number	[-]	*Subscripts*		
p, P	Pressure	[Pa], [-]	0	Initial	
r, R	Radial coordinate	[m], [-]	1	Droplet	
s, S	Arc length	[m], [-]	2	Substrate	
T, Θ	Temperature	[K, °C], [-]	θ	Azimuthal direction	
t , τ	Time	[s], [-]			
u, U	Radial velocity	[m/s], [-]	*Mathematical Operators*		
v, V	Axial velocity	[m/s], [-]	D_τ	Lagrangian derivative towards dimensionless time	
x_{Sn}	Molar fraction of tin	[-]	d_T	Ordinary derivative towards temperature	
z, Z	Axial coordinate	[m], [-]	$\partial_{R,Z}$	Partial derivative towards dimensionless coordinates R, Z	

SURFACE TENSION AND VISCOSITY CORRELATIONS

Variations in surface tension cause a force acting tangentially to the surface considered. Gradients in surface tension originate from (den Boer [8])

- a temperature gradient, causing a thermocapillary effect
- a concentration gradient, causing a destillocapillary effect
- an electrical potential

Since Sn63Pb is an eutectic alloy, we concentrate in the following on the thermocapillary effect, assuming that neither a marked concentration gradient through a non-eutectic solidification nor an electrical potential is involved in the solder droplet deposition process.

The most widely accepted correlation between surface tension γ and temperature is the following linear approach:

$$\gamma = \gamma_{ref} + \left(d_T \gamma\right)_{ref} \left(T - T_{ref}\right) \tag{1}$$

The use of a first order Taylor expansion for the surface tension matches experimental data quite well, in particular if the reference point for determining the surface tension gradient $\left(d_T \gamma\right)_{ref}$ is chosen appropriately within the parametric domain.

Experimental data show a simple exponential dependence of the viscosity μ on temperature. Koke [9] discussed a more sophisticated approach for viscosity especially for alloys, in particular solder. It is based on the work of Thresh and Crawley [10] and can be cited as follows:

$$\mu_{Solder} = \mu_{Pb} + x_{Sn}\left(\mu_{Sn} - \mu_{Pb}\right) \tag{2}$$

where

$$\mu_{Sn} = 2.75 \cdot 10^{-5} \rho_{Sn}^{1/3} \, exp\left(\frac{0.08849 \cdot \rho_{Sn}}{T + 273}\right)$$

$$\mu_{Pb} = 2.54 \cdot 10^{-5} \rho_{Pb}^{1/3} \, exp\left(\frac{0.0863 \cdot \rho_{Pb}}{T + 273}\right) \tag{2b}$$

$$\rho_{Sn} = 7.142 \cdot 10^{3} - 0.6127 \cdot T$$

$$\rho_{Pb} = 1.109 \cdot 10^{4} - 1.3174 \cdot T$$

This set of equations provides the viscosity of solder in [Pa·s] if the temperature T is inserted in [°C]. It has the advantage towards conventional exponential approaches to provide the most realistic approximation for viscosity especially close to the solidification temperature.

One can show by the virtue of statistical mechanics that the approaches for surface tension and viscosity, which both rely on macroscopic measurable properties, are well supported by theories on the microscopic level. A detailed discussion can be found in Fowler [11] and Born and Green [12]. Based on their work, Egry [13] pointed out that there is a fixed relation between viscosity μ and surface tension γ, since they have similar microscopic origins. This justifies the simultaneous consideration of the temperature dependence of surface tension and viscosity in this study.

The thermophysical properties of solder used and shown in Table 1 are carefully chosen and attuned to several literature sources, [14-16].

Table 1 Thermophysical Properties of Sn63Pb @ 260°C

		Liquid	Solid
Density ρ	[kg/m^3]	8218	8240
Viscosity μ_{ref}	[Pas]	0.002237	-
Surf. Tens. γ_{ref}	[mN/m]	498.53	-
Surf. Tens. Slope $(d_T\gamma)_{ref}$	[N/mK]	$-0.214\cdot10^{-3}$	-
Heat Capacity c_p	[J/kgK]	238	176
Thermal Conductivity k	[W/mK]	25	48
Latent Heat of Fusion L	[kJ/kg]	4.2	4.2
Melting Point T_m	[°C]	183	183

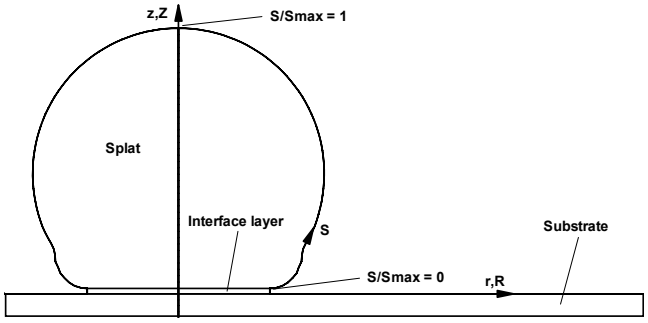

Fig. 1 Schematic of the impingement process

GOVERNING EQUATIONS AND SOLUTION PROCEDURE

Set of Equations

The axisymmetric mathematical description of the problem in a dimensionless Lagrangian form of the Navier Stokes equations is:

Continuity:

$$D_\tau P + \frac{1}{M^2}\left(\frac{1}{R}\partial_R(RU) + \partial_Z V\right) = 0 \tag{3}$$

R-Momentum:

$$D_\tau U - \frac{1}{R}\partial_R(R\overline{\sigma}_{RR}) - \partial_Z\overline{\sigma}_{RZ} + \frac{\overline{\sigma}_{\theta\theta}}{R} = 0 \tag{4}$$

Z-Momentum:

$$D_\tau V - \frac{1}{R}\partial_R(R\overline{\sigma}_{RZ}) - \partial_Z\overline{\sigma}_{ZZ} - \frac{1}{Fr} = 0 \tag{5}$$

Energy, $i = 1$ – Droplet, $i = 2$ – Substrate:

$$D_\tau\Theta_i - \frac{2}{Pe_i}\left[\frac{1}{R}\partial_R(R\partial_R\Theta_i) + \partial_{ZZ}^2\Theta_i\right] = 0 \tag{6}$$

The dimensionless parameters are defined as:

$$\begin{aligned} &R = \frac{r}{d_0}, Z = \frac{z}{d_0}, U = \frac{u}{v_0}, V = \frac{v}{v_0} \\ &\tau = \frac{t}{d_0/v_0}, P = \frac{p - p_{amb}}{\rho v_0^2} \\ &\overline{\sigma}_{ij} = \left(\sigma_{ij} + \delta_{ij}p_0\right)/\rho v_0^2 \\ &\Theta_i = \frac{T_i - min\left(T_{1,0}, T_{2,0}\right)}{T_{1,0} - T_{2,0}} \end{aligned} \tag{7}$$

A sketch of the problem, including the definitions of the coordinates, is shown in Fig. 1. The dimensionless stress components $\overline{\sigma}_{ij}$ in the momentum equations are defined as follows:

$$\overline{\underline{T}} = \begin{bmatrix} \overline{\sigma_{RR}} & \overline{\sigma_{RZ}} & 0 \\ \overline{\sigma_{RZ}} & \overline{\sigma_{ZZ}} & 0 \\ 0 & 0 & \overline{\sigma_{\theta\theta}} \end{bmatrix} \qquad \begin{aligned} \overline{\sigma}_{RR} &= -P + \frac{2}{Re}\partial_R U, \\ \overline{\sigma}_{ZZ} &= -P + \frac{2}{Re}\partial_Z V \\ \overline{\sigma}_{\theta\theta} &= -P + \frac{2}{Re}\frac{U}{R}, \\ \overline{\sigma}_{RZ} &= \frac{1}{Re}\left(\partial_Z U + \partial_R V\right) \end{aligned} \tag{8}$$

where $\overline{\underline{T}}$ is the dimensionless stress tensor. The characteristic dimensionless numbers of the problem are the initial Reynolds, Froude, Mach, Weber and Peclet number defined as:

$$\begin{aligned} &Re_0 = \frac{\rho v_0 d_0}{\mu_0}, \quad Fr = \frac{v_0^2}{d_0 g}, \quad M = \frac{v_0}{c} \\ &We_0 = \frac{\rho d_0 v_0^2}{\gamma_0}, \quad Pe_i = Re_{0i}\cdot Pr_{0i} = \frac{d_0 v_0}{\alpha_i} \end{aligned} \tag{9}$$

where α_i represents the thermal diffusivities of the different regions (i = 1 droplet, i =2 substrate). The dimensionless initial and boundary conditions have the following form:

$$\tau = 0: \begin{cases} U = 0, \quad V = -1, \quad P = \dfrac{4}{We_0}, \\ \\ \Theta_1 = 0, \quad \Theta_2 = 1 \end{cases} \tag{10}$$

$$R = 0: \quad U = 0, \quad \partial_R V = 0, \quad \partial_R\Theta = 0$$

$$Z = 0: \quad U = V = 0$$

The initial substrate temperature is equal to the surrounding temperature and both the free surface of the droplet and the substrate are considered to be adiabatic. The conservation equations (3) – (6) for mass, momentum and energy are spatially discretized with a Galerkin FEM description. The derivatives of the stress tensor components in space can be avoided and change into a projection of the stress tensor onto the outer surface normal. Circumventing these

derivatives, a variable viscosity can easily be incorporated by employing a local Reynolds number for each element, no additional term is introduced in the numerical form of the momentum equations. The local Reynolds number is simply defined as:

$$Re = \frac{\rho v_0 d_0}{\mu} \tag{11}$$

where the local viscosity μ is computed using Eq. (2).

The weak formulation of the momentum equations is:

$$\int_\Omega \phi_k D_\tau \vec{V} + \underline{\underline{\overline{T}}} \cdot \nabla \phi_k + \phi_k \cdot \begin{pmatrix} \overline{\sigma}_{\theta\theta} / R \\ 1/Fr \end{pmatrix} d\Omega = \int_{\partial\Omega} \phi_k \cdot \vec{n} \cdot \underline{\underline{\overline{T}}} d\Gamma \tag{12}$$

For elements at the free surface, the right hand side of Eq. (12) can be rewritten according to Landau and Lifshitz [17]:

$$\vec{n} \cdot \underline{\underline{\overline{T}}} = -2 \frac{\overline{H}}{We} \vec{n} + \frac{\nabla \gamma}{\rho v_0^2} \tag{13}$$

This formulation includes a variable surface tension, since a variable Weber number *We* and an additional surface tension gradient term is introduced. $\overline{H} = H/d_0$ is the dimensionless curvature, where H is given by:

$$H = \frac{1}{r} \frac{z'}{2 \cdot \left[(r')^2 + (z')^2 \right]^{1/2}} + \frac{\left(r'z'' - z'r'' \right)}{2 \cdot \left[(r')^2 + (z')^2 \right]^{3/2}} \tag{14}$$

The primes in Eq. (14) indicate differentiation of the coordinates r and z with respect to the arc length s of the free surface.

Using Eq. (1), the dimensionless temperature Θ and introducing the Marangoni number *Ma*, Eq. (16), Eq. (13) becomes:

$$\vec{n} \cdot \underline{\underline{\overline{T}}} = -2 \frac{\overline{H}}{We} \vec{n} + \frac{Ma}{Re_0} \nabla \Theta \tag{15}$$

$$Ma = \frac{Re_0}{We_0} \frac{\left(d_T \gamma \right)_{ref} \left(T_{1,0} - T_{2,0} \right)}{\gamma_0} \tag{16}$$

The Weber number *We* in Eq. (15) differs from the initial Weber number We_0 expressed in Eq. (9) and has to be defined locally like the local Reynolds number. With Eq. (1) one finds:

$$\frac{1}{We} = \frac{\gamma}{\rho d_0 v_0^2} = \frac{1}{We_{ref}} + \frac{Ma}{Re_0} \left(\Theta - \Theta_{ref} \right) \tag{17}$$

The moving contact line is modeled by applying the Navier-slip condition at the contact line, Baer and Cairncross *et al.* [18]:

$$\vec{n} \cdot \underline{\underline{\overline{T}}} \cdot \vec{t} = \frac{1}{\varepsilon} \vec{V} \cdot \vec{t} \tag{18}$$

In Eq. (18), $\vec{n}$ and $\vec{t}$ are the normal and tangential unit vectors, respectively. The Navier-slip length ε is assumed to be of the order $O(10^{-3})$ as stated in the same reference. One has to keep in mind that this condition only limits the fluid stresses at the contact line. The dependence of wetting on temperature is not modeled.

The solidification process was numerically modeled by setting the velocities to zero when a grid point reached the solidification temperature. The release of the latent heat of freezing was incorporated utilizing the '*exact specific heat method*', Bushko and Grosse [19]. An inert gas atmosphere was assumed to suppress oxidation of the free surface, as it is indeed the case in solder jetting (free surface oxidation would effect the Marangoni convection as mentioned by Arafune and Sugiura *et al.* [20]).

Numerical Solution Procedure

Linear shape functions $\phi_k, k = 1,2,3$ and triangular elements were employed for the spatial discretization. The grid was created with the commercial meshing tool Hypermesh®. An automatically initiated remeshing was executed if one of the internal element angles β_i exceeded the range of $15° < \beta_i < 130°$ through distortion during the transient impact process. The Bach-Hassager iterative scheme was used for solving the fractional time step of Eqs. (3) – (5), describing the fluid mechanical behavior, Bach and Hassager [21]. Convergence was considered as being reached in the fluid mechanical part, when the relative change of the velocities and pressure values were less than 0.1 percent from one iteration to the next. The energy equation (6) was solved as a sub-step, based on the velocities obtained at the end of the fluid mechanical sub-step, using the Crank-Nicholson scheme. To account for the coupling of momentum and energy equation through the dependence of surface tension and viscosity on temperature, the dimensionless maximum time step was chosen with 10^{-4} sufficiently small to avoid unacceptable errors in both, the fluid mechanical and the thermal solution. A further reduction of the time step to decrease the maximal possible surface tension and viscosity change within one time step did not show improved results but strongly increased the needed computing time.

All simulations were performed using a fine grid of about 6500 elements. The average dimensionless element length was about 0.02, which is 1/200 of the initial droplet diameter. This high refinement was chosen to resolve even the smallest changes in spreading behavior, requiring a total CPU time of about 28 h (1 GHz, Pentium III) to complete 50,000 time steps. A number of simulations were performed in order to ensure mass and energy conservation. For the mesh density and the time step utilized, both mass and energy were conserved within less than 1% of the initial values. Furthermore, it was verified that mesh and time step independent solutions were obtained.

RESULTS AND DISCUSSION

Parameter variations

In order to investigate the effects which the temperature dependence of surface tension and viscosity has on the spreading, the transient behavior as well as on the end shape of the droplet, simulations were performed utilizing different values of droplet superheat.

Table 2 Parameter Variations in Simulations

Run	$\mu = f(T)$	$T_{1,0}$	Re_{ref}	We_{ref}	Ma_{ref}
A1	No	200°C	360.97	2.8927	0
A2	No	200°C	360.97	2.8927	-9
A3	Yes	200°C	360.97	2.8927	-9
B1	No	250°C	427.65	2.9545	0
B2	No	250°C	427.65	2.9545	-13
B3	Yes	250°C	427.65	2.9545	-13
C1	No	300°C	491.85	3.019	0
C2	No	300°C	491.85	3.019	-19
C3	Yes	300°C	491.85	3.019	-19
D1	No	350°C	552.78	3.0864	0
D2	No	350°C	552.78	3.0864	-25
D3	Yes	350°C	552.78	3.0864	-25
E1	No	400°C	610.25	3.1569	0
E2	No	400°C	610.25	3.1569	-33
E3	Yes	400°C	610.25	3.1569	-33
F1	No	450°C	664.98	3.2307	0
F2	No	450°C	664.98	3.2307	-40
F3	Yes	450°C	664.98	3.2307	-40
G1	No	500°C	716.17	3.308	0
G2	No	500°C	716.17	3.308	-49
G3	Yes	500°C	716.17	3.308	-49

The initial droplet temperature was changed from 200°C to 500°C in steps of 50K, causing other parameters to change as well, according to their definition in the previous sections. The droplet impact velocity was kept constant at 1.5 m/s. The initial droplet diameter also remained unchanged at the typical value for solder jetting of 80 μm. However, due to the change of the initial droplet temperature, the initial Reynolds, Weber and most importantly the Marangoni number changed from case to case. Table 2 summarizes the simulations performed and the corresponding parameter values.

Influence of Thermal Marangoni Effect

Considering the droplet post-solidification shapes in Fig. 2, every figure compares the end shapes of three cases: One with constant (independent of temperature) surface tension and viscosity (bold dotted line), one involving only the Marangoni effect (thin dashed line) and the third accounting for both, a change of surface tension and viscosity with temperature (bold solid line). The spreading for the constant property cases increases slightly with droplet superheat but is practically constant. This has to be expected since the increasing wettability with higher temperature is not modeled by the Navier-slip boundary condition as mentioned earlier. On the other hand, the spreading decreases by approximately 20% (and with this the contact area by up to 34%) between 200°C and 500°C initial droplet temperature if a variation of both properties with temperature is included, Fig. 2. The change of viscosity has a marginal influence on spreading as can be seen comparing the case of a variable surface tension and a constant viscosity and the case with both thermophysical properties as a function of temperature. Indeed, plotting the contact line radius *x-contact* versus the absolute Marangoni number, *-Ma*, shows a monotonic decrease of the spread radius with increasing Marangoni effect, Fig. 2 h). This clearly indicates that the thermocapillary forces cause the reduced spreading. The change in spreading also influences the final shape of the droplet: The end shapes for the constant property cases are wider and flatter, whereas the final shapes for the temperature dependent properties are narrower and taller.

The reduced spreading with increasing absolute Marangoni number is a counter-intuitive result. One can easily verify with Eq. (15) that the direction of the Marangoni force points towards the substrate, since the Marangoni number is negative and the temperature gradient is positive. One would expect a surface flow in the direction of the contact line, thereby accumulating mass and actually enhancing the spreading. In fact the opposite is observed, spreading is reduced. To further clarify this counter-intuitive result and the influence of the Marangoni effect on the droplet spreading, a detailed investigation of the vorticity evolution ω inside the droplet was performed. For the case without Marangoni effect, there exist two counter-rotating vorticity areas close to the substrate. Fig. 3 a) provides thereby the location of the magnified area shown in Fig. 3 b) within the droplet domain. The vorticity at the free surface is slightly positive for this case, Fig. 3 b). The vorticity of the fluid in the wall region is always negative for all cases, independent whether the Marangoni effect is incorporated or not. These counter-rotating vorticity regions entrain fluid, which they squeeze and direct towards the contact line region, as it can be seen in the illustration on the left hand side of Fig. 3 a). On the other hand, the positive vorticity at the free surface cannot be seen in the case accounting for a Marangoni effect: Figure 3 c) shows the vorticity field for Ma = -49 at the same time step as in Fig. 3 b), τ = 0.3. Thermocapillary forces weaken therefore the effect of fluid entrainment to the contact line, since the vorticity at the free surface in the contact area is changed to negative values. The clockwise rotation of the flow in this case acts against the oncoming inertia flow, hence opposing the radial flow. This mechanism causes a reduction in droplet spreading as observed in Fig. 2.

Considering the freezing time of the contact line (i.e. the time when the contact line is arrested by freezing) in Fig. 4 a), one can see that the contact line is still moving up to three times longer for the highest absolute Marangoni number compared to the lowest absolute Marangoni number. Again, the effect of variable viscosity is not significant. On the other hand, this increase in arrest time of the contact line is less distinct for the cases excluding the Marangoni effect, Fig. 4 b). This leads to the assumption that the strong surface vorticity caused by the Marangoni effect close to the substrate extends the motion of the contact line to longer times. This statement is supported by Fig. 5, showing the temporal contact line evolution for the highest superheat temperature. The spread radius for cases with and without Marangoni effect has an almost identical development until time τ = 0.5. It is only for the Marangoni cases that the recoiling leads to a strong receding of the droplet and to a reduction of the spread radius. Hence, the thermocapillary forces seem to promote this droplet receding during recoiling.

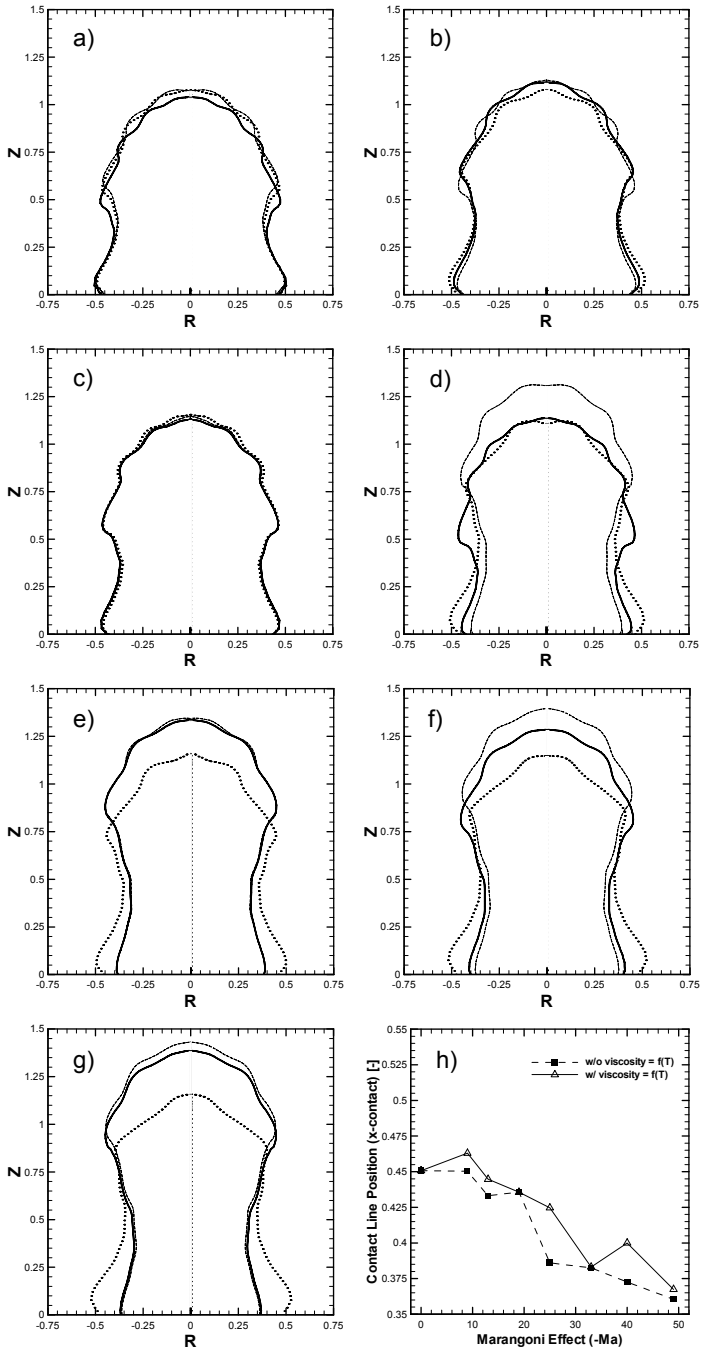

Fig. 2 **Change of spreading with increasing droplet superheat**

a)-g) **Droplet superheat 200°C – 500°C, variation in steps of 50K (see Table 2)**

Bold dotted line: **Constant viscosity and surface tension**

Thin dashed line: **Constant viscosity and variable surface tension**

Bold solid line: **Variable viscosity and surface tension**

h) **Spreading versus absolute *Ma*-number**

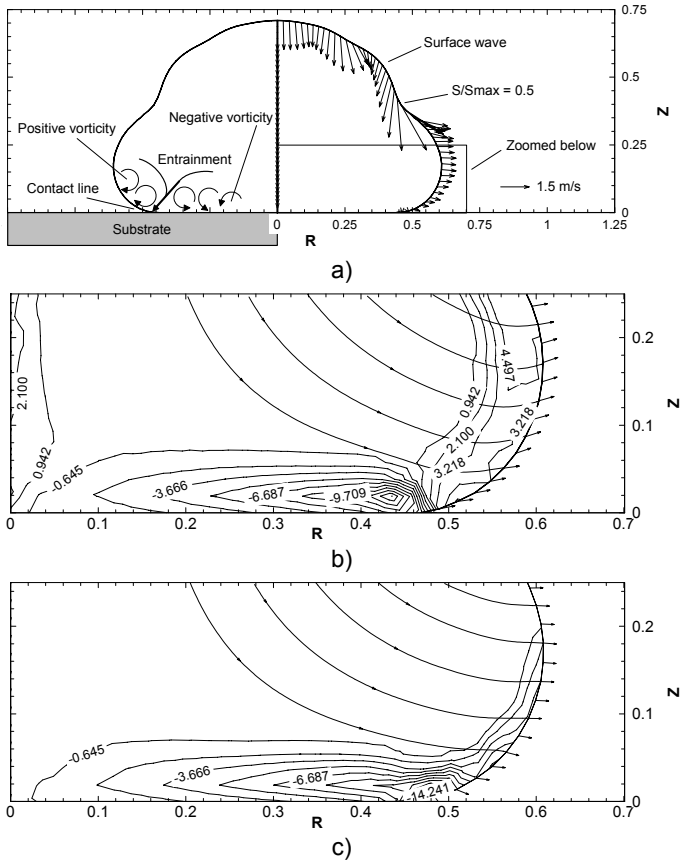

Fig. 3 **a) Illustration of fluid entrainment**
b) Vorticity field without and
c) with Marangoni effect at dimensionless time 0.3

Table 3 reports the mechanism found for the contact line arrest (end of spreading) for different Marangoni numbers. Freezing stops spreading for the cases with small absolute Marangoni numbers since no significant recoiling occurs. This is the same behavior as for cases without the Marangoni effect and therefore expected to eventuate. In contradiction, the stronger thermocapillary forces for larger absolute Marangoni numbers lead to a strong droplet recoiling after the first spreading and especially before freezing can occur. Surface tension forces limit therefore the spreading for larger absolute Marangoni numbers instead of freezing.

As outlined in the previous paragraph, the Marangoni effect influences primarily the droplet spreading and the initial recoiling phase, until the dimensionless time is approximately 1.0. Figure 6 shows the temporal evolution of surface tension from $\tau = 0.1$ to $\tau = 1$ along the surface length for the case of variable surface tension and viscosity and for the highest superheat temperature. It is demonstrated that a noticeable temperature gradient exists primarily only close the substrate, initially imposed by the boundary conditions. The droplet temperature and with it the surface tension are approaching uniform values as time increases. This corresponds to a progressively decreasing Marangoni effect.

Table 3 Reason for contact line arrest

Ma	Contact line arrest due to freezing	Contact line arrest due to surface tension
0	●	
-9	●	
-13	●	
-19	(●)	(●)
-25		●
-33		●
-40		●
-49		●

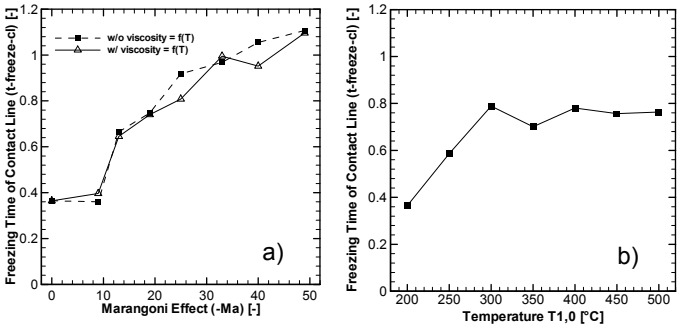

Fig. 4 a) Contact line arrest with and b) without Marangoni effect

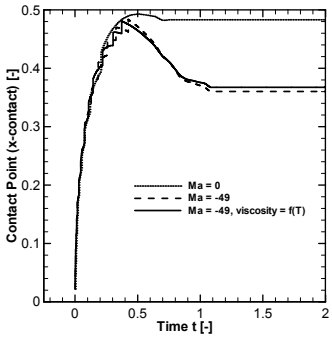

Fig. 5 Contact line evolution for Ma = -49

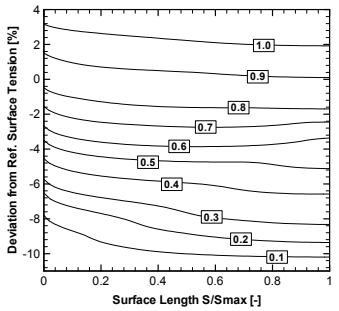

Fig. 6 Surface tension evolution for Ma = -49

CONCLUSION

A numerical investigation was presented, studying the effects of thermocapillarity and viscosity variation with temperature for the deposition of picoliter size solder droplets on a flat substrate. Properties of eutectic Sn63Pb were employed in this study because of its wide spread use for electrical joints. Counter-intuitively, a reduced spreading with increasing absolute Marangoni number was found (the surface tension maximum occurs in the region of the contact line). This finding was explained through the emergence of strong negative vorticity at the free surface in the contact area instead of the moderate positive vorticity observed when no thermocapillary forces were present. Previous studies of a monotonic droplet spreading without initial inertia showed in principal the opposite behavior. Hence, one should not in general study inertia and thermocapillary effects on droplet spreading separately and then superimpose the solutions. The motion of the contact line in time was shown to be a function of the Marangoni number as well. The contact line was arrested due to surface tension forces for large absolute Marangoni numbers, whereas spreading was limited by the onset of freezing for small absolute Marangoni numbers. Thermocapillary forces support droplet receding after the initial spreading, which also leads to a stronger recoiling phase. The final post-solidified droplet shapes were shown to be narrower and taller for large absolute Marangoni numbers (smaller contact area affecting bonding) compared to the constant surface tension cases. The effect of viscosity variation was found to be minor.

REFERENCES

[1] Maronnier, V., Picasso, M. and Rappaz, J., 1999, "Numerical Simulation of Free Surface Flows", Journal of Computational Physics, **155**, (2), pp. 439-455

[2] Haferl, S., Butty, V., Poulikakos, D., Giannakouros, J., Boomsma, K., Megaridis, C. M. and Nayagam, V., 2001, "Freezing Dynamics of Molten Solder Droplets Impacting onto Flat Substrates in Reduced Gravity", International Journal of Heat and Mass Transfer, **44**, (18), pp. 3513-3528

[3] Attinger, D., Zhao, Z. and Poulikakos, D., 2000, "An Experimental Study of Molten Microdroplet Surface Deposition and Solidification: Transient Behavior and Wetting Angle Dynamics", Journal of Heat Transfer-Transactions of the Asme, **122**, (3), pp. 544-556

[4] Cao, C. D., Wang, N., Wei, B. B. and de Groh, H. C., 1999, "Rapid Solidification of Ag-Si Eutectic Alloys in Drop Tube", Progress in Natural Science, **9**, (9), pp. 687-695

[5] Song, S. P., Dailey, P. and Li, B. Q., 2000, "Effects of Heat Source Arrangements on Marangoni Convection in Electrostatically Levitated Droplets", Journal of Thermophysics and Heat Transfer, **14**, (3), pp. 355-362

[6] Ehrhard, P. and Davis, S. H., 1991, "Nonisothermal Spreading of Liquid-Drops on Horizontal Plates", Journal of Fluid Mechanics, **229**, pp. 365-388

[7] Braun, R. J., Murray, B. T., Boettinger, W. J. and McFadden, G. B., 1995, "Lubrication Theory for Reactive Spreading of a Thin Drop", Physics of Fluids, **7**, (8), pp. 1797-1810

[8] den Boer, A. W. J. P., 1996, "Marangoni Convection: Numerical Model and Experiments", Technische Universiteit Eindhoven, Eindhoven

[9] Koke, J., 2001, "Rheologie Teilerstarrter Metalllegierungen", RWTH Aachen, Aachen

[10] Thresh, H. R. and Crawley, A. F., 1970, "The Viscosities of Lead, Tin and Pb-Sn Alloys", Metallurgical Transactions, **1**, pp. 1531-1535

[11] Fowler, R. H., 1937, "A Tentative Statistical Theory of Macleod's Equation for Surface Tension, and the Parachor", Proceedings of the Royal Society of London Series a-Mathematical Physical and Engineering Sciences, **A159**, (896), pp. 229-246

[12] Born, M. and Green, H. S., 1947, "A General Kinetic Theory of Liquids", Proceedings of the Royal Society of London Series A- Mathematical Physical and Engineering Sciences, **190**, (1020), pp. 455-474

[13] Egry, I., 1993, "On the Relation between Surface-Tension and Viscosity for Liquid-Metals", Scripta Metallurgica Et Materialia, **28**, (10), pp. 1273-1276

[14] Keene, B. J., 1993, "Review of Data for the Surface-Tension of Pure Metals", International Materials Reviews, **38**, (4), pp. 157-192

[15] White, D. W. G., 1971, "Surface Tensions of Pb, Sn, and Pb-Sn Alloys", Metallurgical Transactions, **2**, (11), pp. 3067-3071

[16] Carroll, M. A. and Warwick, M. E., 1987, "Surface-Tension of Some Sn-Pb Alloys .1. Effect of Bi, Sb, P, Ag, and Cu on 60sn-40pb Solder", Materials Science and Technology, **3**, (12), pp. 1040-1045

[17] Landau, L. D. and Lifshitz, E. M., 1959, *Fluid Mechanics*, Pergamon Press, Oxford; New York, Vol. 6, pp. 238-241

[18] Baer, T. A., Cairncross, R. A., Schunk, P. R., Rao, R. R. and Sackinger, P. A., 2000, "A Finite Element Method for Free Surface Flows of Incompressible Fluids in Three Dimensions. Part II. Dynamic Wetting Lines", International Journal for Numerical Methods in Fluids, **33**, (3), pp. 405-427

[19] Bushko, W. and Grosse, I. R., 1991, "New Finite-Element Method for Multidimensional Phase-Change Heat-Transfer Problems", Numerical Heat Transfer Part B-Fundamentals, **19**, (1), pp. 31-48

[20] Arafune, K., Sugiura, M. and Hirata, A., 1999, "Investigation of Thermal Marangoni Convection in Low- and High- Prandtl-Number Fluids", Journal of Chemical Engineering of Japan, **32**, (1), pp. 104-109

[21] Bach, P. and Hassager, O., 1985, "An Algorithm for the Use of the Lagrangian Specification in Newtonian Fluid-Mechanics and Applications to Free-Surface Flow", Journal of Fluid Mechanics, **152**, (MAR), pp. 173-190